Buckling-induced zebra stripe patterns in nematic F-actin

Brian Gentry, David Smith, and Josef Käs
Universität Leipzig, Linnestrasse 5, Leipzig 04103, Germany

(Received 24 September 2008; revised manuscript received 8 December 2008; published 25 March 2009)

Rather than forming a simple and uniform nematic liquid crystal, concentrated solutions of semiflexible polymers, such as F-actin, have been observed to display a spatially periodic switching of the nematic director. When observed with polarization microscopy, these patterns appear as alternating light and dark bands, often referred to as zebra stripe patterns. Zebra stripe patterns, although not fully characterized, are due to periodic orientation distortions in the nematic order. We characterize such patterns by using a combination of two techniques. Using polarization microscopy, we quantify the periodic orientation distortions and show that the magnitude of the order parameter also varies periodically in the striped domains. When using fluorescently labeled filaments as markers, filaments spanning the striped domains are seen to undergo large angle bends. With fluorescence, clear density differences between adjacent stripes are also observed with domains of lesser density corresponding to strongly bent filaments. By directly comparing patterned areas with both polarization and fluorescence techniques, we show that periodic variation in the orientation, order parameter, filament bending, and density are correlated. We propose that these effects originate from the coupling of orientation and density that occurs for highly concentrated solutions of long semiflexible polymers subject to shear flows, as previously proposed [P. de Gennes, Mol. Cryst. Liq. Cryst. (Phila. Pa.) **34**, 177 (1977)]. After cessation of shearing, strong interfilament interactions and high compressibility can lead to periodic buckling from the relaxation of filaments stretched during flows. The characterization of zebra stripe patterns presented here provides evidence that buckling in confined F-actin nematics produces strong periodic bending that is responsible for the observed features.

DOI: 10.1103/PhysRevE.79.031916 PACS number(s): 87.16.Ka, 82.35.Pq, 82.35.Lr

I. INTRODUCTION

Actin is an abundant cytoskeletal protein that ubiquitously occurs in eukaryotic cells and is crucial for both cell structure and motility [1–3]. Actin filaments comprise several types of cellular networks found in the cytoskeleton, such as the well-studied dense brushlike structures of the lamellipodium. In addition, actin filaments are often found in tightly packed parallel structures, as in filopodia, stress fibers, microvilli, and hair cells [4]. These cytoskeletal networks play important roles in maintaining a cell's structural integrity, producing forces for protrusion and contraction, and are the origin of other features such as viscoelasticity and the nonlinear response to mechanical stresses [2,5–9].

Because of its importance to cells, the actin protein has been extensively studied and the reaction kinetics and physical properties of individual filaments are well understood. Monomeric actin, or G-actin, polymerizes *in vitro* into long thin helical filaments. Once polymerized, actin filaments are approximately 7–8 nm in diameter and have a polydisperse length distribution over the range of 1 to several tens of micrometers. The length distribution is exponential, with a mean length of 6–7 μm [10].

The mechanical and dynamic properties of filamentous actin (F-actin) in solution are well described by the wormlike chain (WLC) model [11,12]. The model allows the calculation of correlation and response functions, providing a comprehensive framework for the experimental study of mechanical and dynamic properties of biopolymers such as F-actin [13–16]. The defining material properties of WLCs are the intrinsic bending stiffness κ_f and the persistence length given by $L_p=\kappa_f/k_BT$. L_p is the distance over which thermal bending fluctuations become uncorrelated, which is ~ 9 μm for F-actin in the absence of other actin-binding proteins and ~ 18 μm when stabilized with phalloidin [17,18]. Because typical filament lengths $L \sim L_p$, F-actin is considered to be a semiflexible polymer.

Another interesting property of F-actin is its ability to form a lyotropic nematic liquid crystalline phase above a threshold concentration. This spontaneous long-range orientational order is entropy dependent and directly related to its elastic rodlike properties. Since nematic liquid crystal phases have lower symmetry than isotropic phases, they require additional means to characterize their directionality. Macroscopically, this is accomplished by the introduction of the director, which characterizes the spontaneous ordering along the direction of the long axes of the filaments themselves typically treated as rigid rods or cylinders. The director is represented by the headless vector **n**. Microscopically, the anisotropic nature of rigid rods requires an additional parameter to quantitatively characterize the degree of ordering around the direction of the director [19,20]. This quantity, known simply as the order parameter, must take into account the cylindrical symmetry of the angular distribution function of the rods within a given system and the equivalence of **n** and **−n** [21]. The result is an expression for the distribution of rods about the director,

$$S = \frac{1}{2}\langle 3\cos^2\theta - 1\rangle, \tag{1}$$

where θ is the angle between a given rod and the director. For cylindrical rods, this results in a range of the degree of alignment from $S=0$, representing entirely random orienta-

tions, to $S=1$, representing completely parallel alignment [20].

The characteristics of F-actin liquid crystal polymer systems, including onset concentration, effects of length distribution, and rheological, thermodynamic, and optical properties have been the subject of a number of investigations [22–27]. A recent study has shown that the onset concentration for intrinsic nematic ordering of actin filaments occurs between 75 and 150 μM rather than between 25 and 50 μM, as previously reported [27]. At these concentrations, the ordering is thermodynamic in origin. Below this limit, nematic ordering has been observed *in vitro*, but its cause stems from mechanical stresses in the samples which are typically confined in capillaries or between microscope slides [27].

In a majority of nematic actin research, no evidence of the theoretically predicted miscibility gap in which isotropic and nematic domains coexist has been seen [22–24,27]. Polydisperse nematic actin solutions do not fully demix and, therefore, do not macroscopically phase separate, likely due to their high viscosities. Actin nematics are instead comprised of many distinct domains of different orientations that seem to depend on the mechanical history of the sample [23,27]. However, recent studies have shown that the nature of the phase transition is highly length dependent and that, in fact, an authentic first-order transition occurs for systems containing filaments with lengths of 2 μm or less [28]. Above this value of filament length, the phase transition appears to be continuous [29,30].

The parallel alignment of actin filaments along their long axes in the nematic phase results in an observable optical birefringence. This birefringence can be utilized, via polarization microscopy, to discern the direction of alignment or director of domains of different orientation in thin samples. With more advanced techniques, it can also be used to calculate the order parameter within a sample. Reports utilizing conventional polarization microscopy in order to determine the direction of the director have shown that confined nematic F-actin systems display "polycrystalline" textures due to small distortions in the director [22–27,30]. Such textures have been observed in conventional nematics as well and are reported as due to the sensitivity of the alignment of the polymers to mechanical disturbances. It has been proposed that small fluctuations of mechanical forces cause local director orientation distortions and the boundaries between domains of different orientations result in discontinuities in observable optical properties [31].

Among the textures seen in nematic actin samples, periodic striped patterns of alternating birefringence intensity, as observed in polarization microscopy, have attracted some attention [22–26]. Because high-resolution images were either not available or not included, and no standardized descriptive terminology exists, it is often difficult to ascertain if these studies definitely refer to the same phenomenon. Nevertheless, from a survey of this literature, a distinction can be made between a larger-scale flow-induced property characteristic of nematic liquid crystal polymers in which large bands form from a twisting of the nematic director, termed "twisted" or "helicoidal" [24] and the so-called "zebra stripes." The former are typically oriented in the direction of flow and have a swirled helicoidal appearance suggestive of turbulent flow. The latter refer to an ordering of the nematic into textures comprised of fine striations oriented perpendicular to the putative direction of flow (or the nematic director **n**) that indicate a periodic alteration of the director and are generally much smaller than the large swirls referred to in the former case. It is the second case which is of interest in this study.

The origin of zebra stripe patterns has not been elucidated, although some speculations have been put forth based on experimental evidence and by comparison to other liquid crystalline nematics. Both active processes [24] and shear effects [22,25,26] have been reported as the causes of the patterns. Other thermotropic and lyotropic polymers are known to form zebra patterns as a result of relaxation processes at the end of a shear [32–36]. Das *et al.* [26] speculated that a similar mechanism is at work in actin nematics and further presumed that these structures do not owe their stability to being equilibrium states in the presence of special surface or boundary conditions, but rather to the high viscosity and long relaxation times of these polymer solutions.

In this study we investigated zebra stripe patterns in highly concentrated F-actin solutions using an advanced polarization microscope that offers substantial improvement over previous techniques. With this method, we were able to quantitatively determine the periodic orientation distortions in the nematic director that characterize these patterns. In addition, we found that the order parameter also varies periodically in the striped domains. The alignment of the filaments in the domains was directly visualized using a small number of labeled filaments as markers, giving clear demarcation to the boundaries between patterned and nonpatterned areas. We observed long filaments that spanned the stripes and were bent through large angles in order to follow the direction of orientation distortions. In addition, clear density differences that were coupled to the periodic orientation distortions were observed. A direct comparison was made of a patterned area with both polarization and fluorescence, revealing unique properties of this phenomenon. We have shown that periodic variation in the orientation, order parameter, filament segment configuration, and density are all correlated.

Additionally, we explored possible mechanisms underlying the formation of these zebra stripes. In particular, energy dissipation and active processes involving coupling of distortions in the orientation of the nematic director to actin's reaction kinetics were considered, but conclusive evidence indicating these as an underlying cause was not found. Instead, a buckling instability that results from relaxation of flow-induced distortions seems more likely. We present a description of the origin of buckling in the nematic and a plausible mechanism for the subsequent periodic order parameter and density heterogeneities coupled to this process.

II. MATERIALS AND METHODS

A. Sample preparation

1. Actin purification and concentration

G-actin was prepared from rabbit muscle according to the method of Pardee and Spudich [37] purified by gel filtration

chromatography using a Superdex HiLoad 26/20 prep grade column (Amersham Biosciences) and its concentration determined using a Beckman DU 530 spectrophotometer. 10 ml of G-actin at approximately 50 μM were typically produced in these preparations. The protein was stored in G-buffer (5 mM Tris, 0.1 mM $CaCl_2$, 0.2 mM ATP (adenosine triphosphate), 1 mM DTT (dithiothreitol), and 0.01% NaN_3) overnight on ice for later concentration.

In order to concentrate the monomeric actin, 100 mM KCl and 1 mM $MgCl_2$ were added to the entire yield and it was allowed to polymerize for 1 h at room temperature. The F-actin was then centrifuged at $100\,000 \times g$ for 6 h. The F-actin pellet was resuspended through homogenization in a minimal amount of G-buffer and dialyzed for 24 h against the same. The concentration was determined and the concentrated G-actin was then placed in 10 μl aliquots for convenient use in experiments, quick frozen in liquid nitrogen, and stored at $-80\,^{\circ}$C. Due to the relatively large volume of concentrated actin produced and the small volume required for each experiment, it was possible to perform all of the experiments presented here using two different G-actin preparations (although other preparations at different concentrations were used in earlier trials). These were both in the range of 270–280 μM. The monomeric actin from these preparations was diluted with G-buffer to the desired concentrations prior to polymerization for use in the samples.

2. Birefringence samples

Samples were prepared by first adding 4.5 μm polystyrene beads (Polysciences Europe GmbH, Eppelheim, Germany) to the G-actin solution so as to give an average distance of 60–70 μM between beads in the final sample area. These beads were used in order to control the approximate sample thickness by acting as spacers. The G-actin was then polymerized with the addition of 5% KME (0.1 M KCl, 1 mM $MgCl_2$, and 0.2 mM EGTA). The solutions were mixed by gently stirring in a centrifuge tube with a pipette tip in order to avoid filament breakage. 7–10 μl of the final F-actin solution was placed on a microscope slide; a 22×22 mm^2 coverslip with thin coatings ($\sim$3 mm wide) of vacuum grease around the edges was placed on top of the drop and then pressed flat, with care taken to remove trapped air pockets. The slide and coverslip were then pressed together between two aluminum plates in a controlled fashion with a micrometer. It was found that the additional compression did not affect the resulting patterns.

Microscope slide and coverslip surfaces were cleaned with ethanol and washed with Millipore (Millipore GmbH, Schwalbach, Germany) purified water. Both surfaces were initially coated with Sigma-cote (Sigma, St. Louis, MO, USA) in order to prevent nonspecific adsorption of filaments. Because no difference was seen in the patterns with or without Sigma-cote, its use was discontinued.

3. Fluorescence samples

Samples for fluorescence imaging were prepared identically to those above with the following exception. TRITC-phalloidin (Sigma, St. Louis, MO, USA) labeled F-actin was polymerized separately, added to a final concentration of 50 nM, and gently stirred. This concentration was chosen to optimize clear fluorescence imaging (see below). Due to the low ratio of relative concentrations of labeled and unlabeled filaments ($\sim 1/4000$ molar ratio of monomeric actin), no significant concentration-dependent effects on the patterns due to addition of the labeled filaments are expected.

B. Methods of imaging

1. Birefringence

Birefringence measurements were performed on a Leica DM IRB inverted microscope (Leica Microsystems, Wetzlar, Germany) using a 20× objective and equipped with a CRI PolScope apparatus (Cambridge Research, Inc., Worcester, MA, USA). The PolScope utilizes electronically controlled liquid crystalline compensators that avoid the necessity of rotating the sample or polarizers. Computerized control enables an orientation-independent determination of the birefringence magnitude (measured as a retardance) at each pixel position. This represents a substantial improvement over previously used techniques by allowing calculation of birefringence and thus the order parameter with high spatial resolution. In addition, the orientation of the slow axis at a given image point is determined, revealing the local direction of alignment of anisotropic structures within a given sample [38,39]. For F-actin solutions this corresponds to the nematic director **n**. Color coding of the relative orientations within an image enables direct observation of local changes in the director orientation that were previously unavailable. Thus the periodicity of the distortions becomes readily apparent.

2. Fluorescence

Fluorescence measurements were performed with the same microscope using a 40× objective also equipped with a Hamamatsu Orca IEEE 1395 digital charge-coupled device (CCD) camera (Hamamatsu Photonics Deutschland GmbH, Herrsching am Ammersee, Germany). The latter was controlled by LABVIEW (National Instruments, Munich, Germany) software. The amount of fluorescently labeled filaments in the samples was chosen to be diluted enough such that individual polymers could be discerned, yet concentrated enough so that patterns in the unlabeled background could be recognized, similar to previous methods [40,41]. In some cases, the labeled filaments were broken by pipetting or sonication in order to shorten the average length, yielding clearer images.

The use of fluorescent markers revealed local details of filament segment orientation such as nematic splay and periodic bending that is not available with other methods. The use of both techniques for the same area within a single sample provided a direct check of filament orientation within the zebra stripes, as well as a direct comparison of order parameter, filament segment configuration, and local density.

III. RESULTS

In this study, highly concentrated thin actin samples were analyzed with polarization microscopy and characteristic ze-

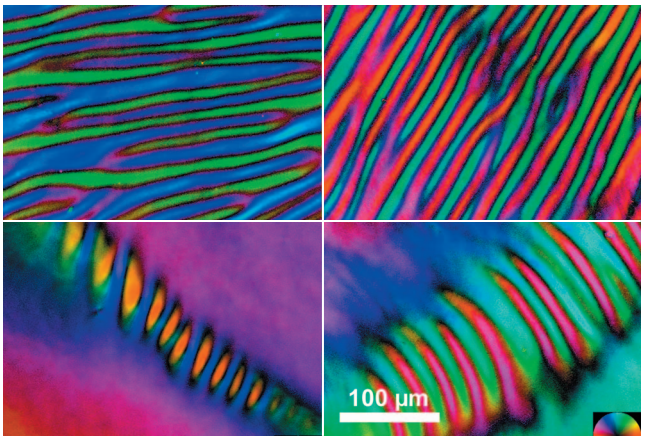

FIG. 1. (Color) Four representative images showing periodic distortions in the orientation of the nematic director as revealed by the PolScope. Local orientation at each pixel is coded by different colors corresponding to the angles relative to the image reference frame. The angles for all four images are given by the color wheel (lower right). They display strong periodicity in which the orientation of the director alternates from stripe to stripe.

bra stripe patterns were observed. The use of the PolScope allowed visualization of the periodic distortions of the nematic director via color coding of the angles relative to the image reference frame. The degree of regularity in the director alterations was remarkable, as seen in Fig. 1. In striped areas, this periodicity was found for all cases regardless of the size, shape, or width of the stripes.

The PolScope also provides a quantitative determination of the local optical retardance in the patterned regions, represented by the grayscale intensity. Thus, the thin black separations observed between regions of different alignments in images displaying the characteristic zebra striped patterns correspond to areas with low retardance or, alternatively, birefringence. Lower birefringence magnitude could be due to the complete absence of filaments, indicating density discontinuities in the nematic, to a lesser density of aligned filaments, or to dense filaments locally displaying no orientational order. It is not possible to differentiate between these possibilities with polarization microscopy alone.

The local optical retardance information obtained by the PolScope was used to calculate the order parameter of the nematic with high spatial resolution. In turn, variations in the order parameter were used to determine a nominal wavelength of the patterns from the periodicity observed in the retardance intensity (Fig. 2, upper left). This was executed in the following steps. First, patterns of similar qualitative appearance were selected. It should be noted that a variety of striped patterns were observed with lines of varying thickness and some variation in shape. There were, however, a large subset of patterns displaying thin regularly spaced stripes and these were selected for wavelength analysis due to their regularity.

For a selected area in a particular image, the retardance intensity profile was determined along a line perpendicular to the stripes. Nine additional profiles parallel to the first but shifted approximately 1 μm in either x or y (Fig. 2, upper left) were then computed. The retardance values were then

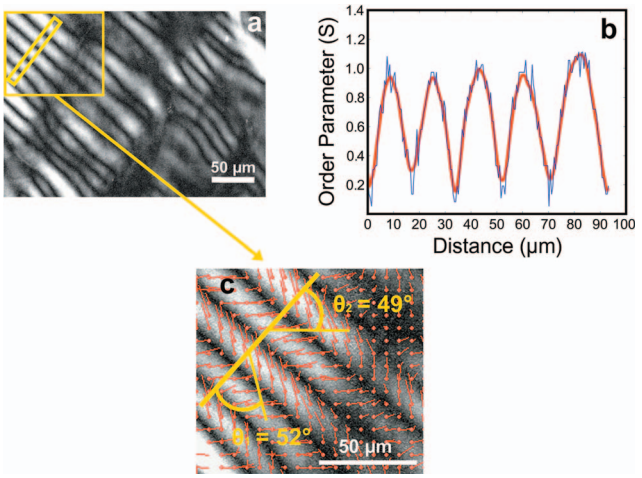

FIG. 2. (Color) Analysis of the periodic variation of the order parameter and distortion angles in striped regions. (a) Striped regions displaying a regular periodicity as seen in the thin rectangular section were chosen for analysis. The specific retardance was determined at each pixel along a line perpendicular to the stripes. From this value, the local order parameter at each point on the line was calculated according to Eq. (2) from the main text. A plot of a single scan is shown in (b). The determination was repeated for nine such parallel lines along the stripe, each separated by approximately 1 μm, and the values for the order parameter were averaged in order to determine the periodic spacing of the stripes. The corresponding angular dependence of the alternating distortion of the local filament orientation in stripes was determined as shown in (c). For the analysis region, the angular difference or distortion angle (θ_1 and θ_2) between the local orientation of the nematic director as determined by the PolScope (red lines) and the reference line used for analysis in (a) and (b) was determined for each stripe. This value was averaged for each of the two alternating orientations to give the average θ_1 and θ_2.

converted to an order parameter by first calculating the specific birefringence according to $\Delta n = r/d$, where r is the retardance value obtained from PolScope images and d is the sample thickness [42]. Then, the order parameter was calculated at each point using the relation

$$S = \frac{\Delta n}{c}(2.3 \times 10^{-5}), \tag{2}$$

where the value $\Delta n_0/c = 2.3 \times 10^{-5}$ ml/mg is a proportionality constant previously determined for optical birefringence measurements and corresponds to a completely aligned F-actin solution [43]. The result for a single scan is shown in Fig. 2, upper right.

In order to determine the pattern wavelength, a Fourier transform was performed on each scan and the wavelength calculated from the largest frequency peak. These values were then averaged over all ten scans. Even with this qualitative preselection of the images, there was considerable variation from image to image with wavelengths in the range of 9–18 μm for the 13 images analyzed.

It is clear from Fig. 2, upper right that the striped domains alternate *continuously* between very highly and very weakly aligned nematic regions. The maximum values are quite

high, between 0.93 and 1.09; the latter of which exceeds the theoretical limit. The order parameter, however, is clearly not higher than unity. This discrepancy can be explained by errors in the sample thickness of only 10%, which could easily account for the overly high values. Assuming such errors places the highest values in agreement with the experimentally determined order parameter saturation value of Viamontes *et al.* [43] for actin solutions above ~5 mg/ml. This value, also obtained using a PolScope, was approximately 0.85.

The minimum values of the order parameter show that the black lines seen between striped domains of different orientations (Fig. 1) correspond to areas of significantly lower nematic alignment. The values, 0.2–0.3, correspond to concentrations of approximately 47–60 μM [43], which approach the onset of nematic ordering. Our results are consistent with the observed continuous increase in birefringence seen above nematic onset and show that the stripes do not result from alternating isotropic and anisotropic domains [29,30]. In addition, the characteristic striped patterns were consistently observed at all concentrations above the putative nematic onset concentration of 45 μM [27]. The concentration of the samples investigated was therefore chosen to assure that they were well above this limit, with typical values of 200 μM.

The POLSCOPE software was also used to analyze the distribution angle of the optical axes of the zebra stripes. The PolScope displays the orientation of the slow axis of the local birefringence at a user-defined frequency, which is interpreted as the local nematic director (see Sec. II B 1). From this information, the angles of the directors relative to the reference lines used above were determined. For each stripe of alternating director, the angle between the director and the reference line was measured in each of the images used in the wavelength analysis. Angles from similarly oriented stripes (e.g., θ_1 in Fig. 2, lower middle) were averaged over the observation region. This angle was termed the "distortion angle" because it describes the local deviation of the nematic director from alignment along the putative undistorted direction within the given region of the liquid crystal.

The PolScope images show considerable variation in the distortion angles between samples and even between different patterned areas within a single sample. In a given region, often spanning 100 μm or more, however, the distortions in the director alternated regularly as seen in Fig. 1. The difference between angles of similarly oriented stripes (θ_1 or θ_2 in Fig. 2, lower middle) was typically $\leq 15°$. As an additional means to characterize the periodicity, the angular shift in directors between neighboring stripes was defined to be $\phi = 180 - (\theta_{1\,\mathrm{avg}} + \theta_{2\,\mathrm{avg}})$. ϕ was found to range between 51° and 84.5°, with an average value of 70.5° for all 13 images used in the analysis. These values of ϕ imply that filaments spanning the stripes would undergo considerable bending.

In order to obtain more detailed information regarding the alignment of individual filaments in the striped regions, fluorescently labeled polymers were added to the unlabeled background at a ratio of ~1/4000. This technique allows direct visualization of the local behavior of an unlabeled background in entangled and liquid crystalline F-actin solutions [40,41], particularly that of the nematic director. In some samples the labeled filaments were shortened by pipetting before addition to the background filaments in order to better visualize individual filament behavior.

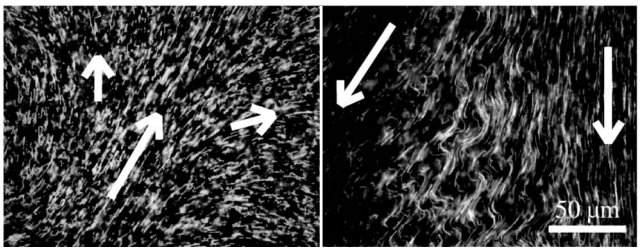

FIG. 3. Two representative images showing direct visualization of splay in the nematic using a small number of fluorescently labeled filaments embedded in a dense unlabeled background. The ratio of labeled to unlabeled filaments in both images is approximately 1/4000. In many of the samples observed, orientation distortions characterized by strong bends in the filaments were associated with the splay (right).

Using this technique, numerous examples of large splay were observed (Fig. 3, left). It was found that areas displaying significant distortion of the nematic director were often associated with nematic splay (Fig. 3, right). In addition, filament contours could be directly visualized in areas of periodic director distortions. There, they exhibited a zigzag pattern and were strongly bent between domains of alternating alignment as they followed the director of the dense unlabeled nematic background (Fig. 4). The strong bending confirms PolScope observations that the angular shift in directors between neighboring stripes would result in large angle bending of filaments spanning the domains.

An estimate of the energy required to bend a single filament by such large angles was obtained from sample images displaying long filaments that spanned the stripes. First, a circle was drawn that corresponded to the arc made by the bent filament segment. From this, a radius of curvature and bending energy were calculated. For the segment shown in Fig. 5, a bending energy of 0.163 kT/μm was obtained. For 26 filaments measured, the bending energies ranged from 0.2–0.7 kT/μm, with an average of 0.5 kT/μm. Thus it can be seen that bending of filaments by the nematic background field has a relatively low energy cost even for large bending. This is well known for nematic polymers, which do

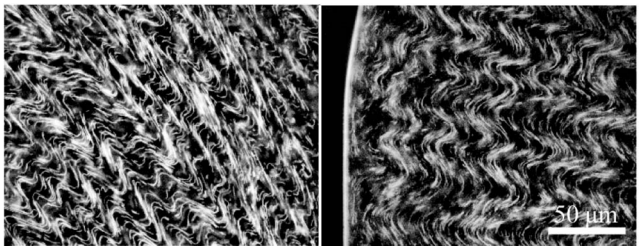

FIG. 4. Two representative images using fluorescently labeled filaments that reveal periodic director distortions. The filament contours display zigzag patterns and show strong bends between bands of alternating alignment. The strong bends in filaments that span the stripes confirm PolScope observations of large angular shifts in directors between neighboring domains.

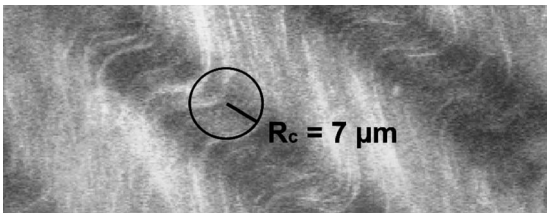

FIG. 5. Representative image of fluorescently labeled filaments used to obtain estimates of the energy required to bend them by large angles. A circle drawn to correspond to the arc made by a bent filament segment is shown in black. The radius of curvature of this circle, and thus of the filament segment, was determined and used to calculate the bending energy in terms of kT/μm.

not require large energy even for hairpin turns [44].

The transition between undistorted nematic alignment and regions with strong periodic director distortions could also be identified by the use of the labeled filaments. A smooth transition from highly aligned nonpatterned to strongly and periodically bent regions was always seen, with no evidence of discontinuity between them (Fig. 6, left).

Another interesting and unique feature observed with this technique was the drastic differences in the fluorescence intensity between adjacent stripes (Fig. 6). These periodic differences in brightness demonstrate strong density heterogeneities that are clearly coupled to the distortions in the direction of the nematic director, in contrast to results from a previous study [30]. Successive stripes appeared alternatively dark and light, with the dark stripes correlated with highly bent filament configurations. Interestingly, stark differences in labeled filament density were observed even in areas of the samples in which only very short labeled polymers were found (Fig. 7). It should be noted that the unlabeled background certainly contained long filaments.

Information from both polarization and fluorescence techniques was also directly compared for a single striped region in order to understand the relation between local filament segment orientation, density, and order parameter. There was a direct match of the filament segment orientations to the color-coded angles shown using the PolScope (Fig. 8). In addition, there was a clear correlation between the periodic distortions of the nematic director with both the density of filaments within the stripes and with the variations in the order parameter calculated from the specific birefringence.

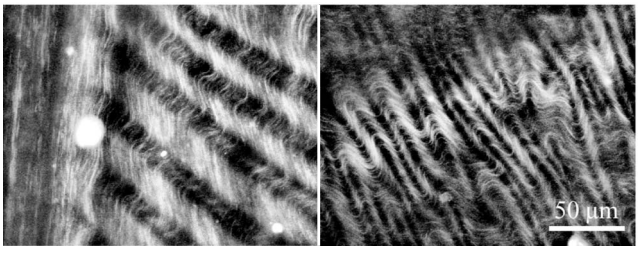

FIG. 6. Two representative images of fluorescently labeled filaments displaying periodic director distortions and showing large differences in filament density between the stripes. Darker stripes of lesser filament density are seen to correspond to regions in which filaments are strongly bent.

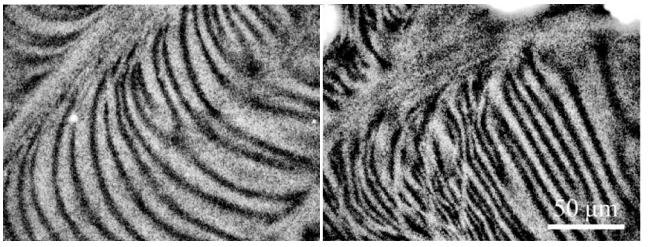

FIG. 7. Two representative images showing periodic distortions in the orientation of the nematic director using fluorescently labeled filaments shortened by sonication before addition to the samples. These images show that even short filaments display significant density heterogeneities. These filaments are presumably small enough to be evenly distributed among the stripes in patterned areas.

From this comparison, it can be seen that regions of high filament density and straight highly aligned filament segment configuration correspond to high birefringence and thus high order parameter, whereas regions of low filament density correspond to low birefringence and low order parameter. Furthermore, the regions of low filament density and low birefringence or order parameter directly correspond to regions of highly bent filament segments *between* the stripes of periodically alternating director orientation. These, in turn, correspond to the thin black stripes observed along the borders of regions of different filament segment orientation in the PolScope images (Fig. 8, left). The relationship between birefringence, order parameter, and density will be discussed in Sec. IV A 2.

The PolScope was used in several experiments designed to test for the possibility that actin reaction kinetics play a causal role in the formation of the zebra stripes. There are two potential causative mechanisms of zebra stripe patterns that could be related to filament polymerization. The first mechanism is based on the reasonable hypothesis that energy consumption by the collective reaction-diffusion mechanism of treadmilling could lead to instabilities that generate pat-

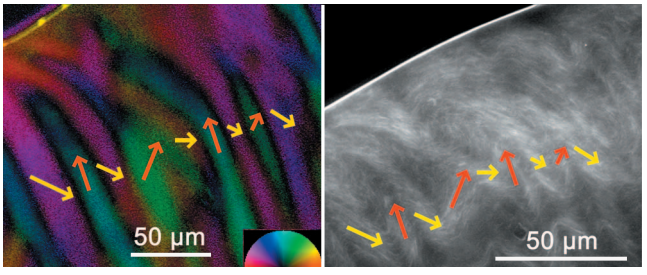

FIG. 8. (Color) Comparison of the same region of a sample using both orientation color-coded polarization (left) and fluorescently labeled filaments (right). Yellow and red arrows indicate the actual orientation of filaments within the stripes obtained with each method. The arrows show a direct match of filament segment orientation between identical domains in the two images. These images also show that the black lines between the stripes observed with polarization (left) match the darker stripes of lesser density using fluorescence (right). From this comparison it can also be seen that the dark stripes in the polarization images correspond to regions of highly bent filaments.

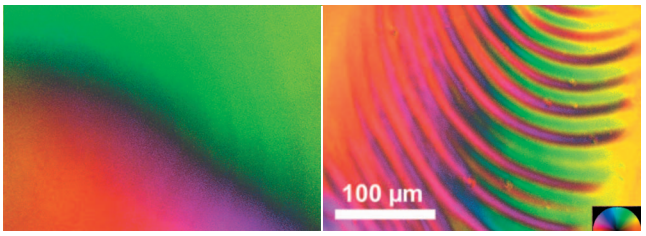

FIG. 9. (Color) Differences observed between samples polymerized under cold conditions (left) and then subsequently sonicated at room temperature for 5 s (right). Under cold conditions, large nematic domains with no zebra stripe patterns were observed. After sonication, patterns were seen throughout the sample. These images show that induced mechanical stress is the mechanism responsible for the pattern formation. Local orientation is coded by different colors corresponding to the angles given in the color wheel (lower right).

terns. Treadmilling F-actin solutions are not in the thermodynamic ground state, which is presumed to be that of an undistorted nematic and not one characterized by striped patterns in which the filaments are strongly bent. Observable nonequilibrium effects such as spatial patterns would therefore indicate that a nonlinear thermodynamic mechanism is at work. The second mechanism involves buckling of growing highly concentrated filaments that result in a periodic warping of the nematic director [24,45]. In this case, filaments jam against one another as they grow in a confined space and they buckle to relieve the accumulated stress.

In order to test the first potential causal mechanism of pattern formation involving actin reaction kinetics, the ATP conditions of the samples were varied. First, ATP in G-actin was depleted using hexokinase and the actin was polymerized in the presence of adenosine diphosphate (ADP). Consistent with a previous study, no difference was seen in the patterns [24]. This result was not surprising given that the available ATP from the G-buffer (Sec. II A) would be quickly depleted by highly concentrated F-actin. Second, in order to test the possible effects of extended treadmilling, additional ATP was added to a final concentration of 25 mM, representing an increase of 125 times that of the typical samples. Again, no difference was seen in the patterns.

The second mechanism was tested by assembling the samples at low temperatures in order to decrease the polymerization rate [46–48]. All solution components and anything contacting the sample were first cooled on ice. Samples were then assembled inside a 4 °C refrigerator to assure no ambient temperature increase. In several samples assembled using this method, no zebra stripes were observed. Instead, large nematic domains of different orientations were seen with black borders at the intersection between regions of different alignments (Fig. 9, left). Upon application of mechanical stress, either by sonication or pressing on the sample, patterns were seen to "instantly" appear (Fig. 9, right). Patterns were never seen to grow or increase in size in the sample. Due to the high protein concentrations of the samples, however, the initial polymerization rate may not have been greatly affected by the temperature decrease, and an alternate explanation is indicated (Sec. IV B 2).

At the high concentrations used in this study, it was found that even G-actin in the absence of polymerizing salts formed striped birefringent patterns near the edges of the sample. The stripes did not extend as far into the body of the sample and were found exclusively at the edges (data not shown). These stripes were presumably due to the formation of short F-actin oligimers in actin solutions whose concentrations were high enough to overcome the energy barrier of the nucleation step and exceed the critical concentration, resulting in short stable filaments [10,48–50].

Additionally, reduction in the average filament length to 5 and 1 μm by addition of gelsolin produced no significant change in the patterns. F-actin solutions of these average lengths at high concentrations, however, have been shown to still be nematic liquid crystals with significant degrees of birefringence [29]. Only when phalloidin was added to the entire sample and it was disrupted by sonication for 10–20 s were the patterns significantly altered or eliminated.

IV. DISCUSSION

A. Characterization of zebra stripe patterns

1. Order parameter variations, strong bending, and density heterogeneities

In this study, we report on experimental findings with nematic F-actin solutions previously not accessible with conventional polarization microscopy that reveal unique local behavior of confined liquid crystalline semiflexible polymers subjected to shear. Analysis of PolScope optical retardance values showed a high degree of local order parameter variation within the striped areas along with a smooth alteration between high and low values of nematic ordering (Fig. 2). Previous studies measuring the birefringence of confined nematic F-actin samples ignored local variations and focused instead on larger regions [27,43]. This resulted in bulk measurements and essentially averaged over these variations. In addition to retardance information, the PolScope also provided direct evidence of large distortion angles of the director between the regularly alternating domains.

The use of fluorescent markers distributed throughout the nematic gel made it possible to directly visualize the filament segment orientation in the patterned areas. This provided detailed information, complementing that obtained from polarization observations. These two techniques lend greater insight into the behavior of these systems. A number of observations were readily apparent from this combined approach. First, the regular periodic distortion of the nematic director as revealed by PolScope polarization images was also seen in the fluorescence images. These patterns of alternating director were also seen to be associated with splay in the nematic.

In addition, large bending angles in long filaments that span the zebra stripes were observed, consistent with the large distortion angles observed with polarization. This demonstrates that the periodic variations of the nematic director are continuous, with the filaments bending to conform to the large distortions. Interestingly, dramatic density heterogeneities were observed in the striped regions that corresponded

to the filament segment configuration. Darker less concentrated areas corresponded to highly bent filament segments and bright more concentrated ones contained very straight segments. A possible explanation for this coupling is given below.

2. Correlation of periodic variations

Direct comparison of zebra stripe regions using both techniques simultaneously shows that order parameter variation, periodic bending of filament segments, and local polymer density are directly related (Fig. 8). We propose that the increased density of the filaments in the straight regions results in an increase in filament ordering and not just an increase in birefringence due to more filaments per given area. This can be understood by the following arguments. Filaments above the entanglement concentration are sterically confined by interaction with surrounding polymers to a tubelike region around the filament contour [21]. It can be assumed that the diameter of the tube confining each polymer segment in these regions is smaller due to the increased density of filaments. This means that the characteristic minimum length between two points where the filaments touches the tube, known as the deflection length, would be smaller [51]. A smaller deflection length would result in a higher order parameter in these regions since appreciable bends transverse to the local nematic director would not occur (i.e., the filaments are, on average, straighter). This conclusion is supported by the fluorescence images, in which the filament segments appear remarkably straight in regions corresponding to high order parameters (e.g., Fig. 4, left).

Another explanation for the higher order parameter in the denser regions is the potential bundling of the filaments. Higher density that results in closer packing, as described above, could cause the filaments to form bundles by electrostatic or steric interaction. It is well known that bundling of bipolymers such as F-actin and microtubules can be induced by such effects [52]. This hypothesis is supported by images containing fluorescently labeled filaments, such as Figs. 3–6, in which the labeled filaments often appear aggregated into thick cables. Bundling and interfilament interaction has recently shown to be important in microtubule systems that also form zebra stripe patterns [45,53]. In these studies, the authors speculated that the combined effects of counterion-induced attraction and depletion force caused the formation of clearly observable microtubule bundles. Their fluorescence images of the microtubules show clearly discernable bundles; however, such a reasonable estimate of bundle thickness could be obtained with an average of 280 microtubules per bundle. Potential F-actin bundles studied in our system appear much thinner and are therefore more difficult to differentiate. It is, nonetheless, reasonable to assume that bundles will form by steric effects given the close confinement of the filaments in such thin sample chambers.

The high degree of quasi-two-dimensional (2D) confinement is also the likely cause of differences between the experiments presented here and those in other reports on F-actin using the same observation techniques [29,30]. In particular, no density differences were seen in [29,30] in samples showing zebra stripes, even though the specific birefringence, local nematic director distortions, and filament concentration were shown. The sample chambers were typically ~40 times thicker, however, so this is a likely explanation for the difference, suggesting that confinement effects in such thin samples is an important factor in this phenomenon.

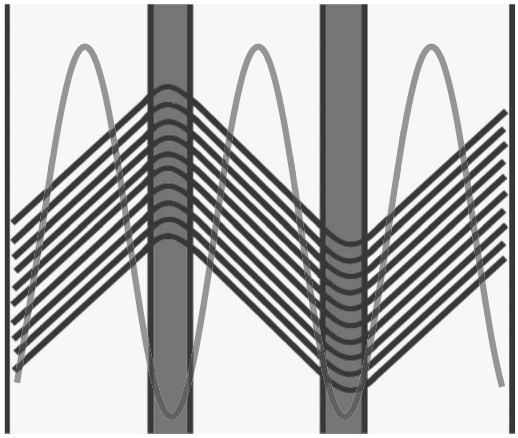

FIG. 10. Diagram showing modified zebra stripe patterns with regions of straight densely packed filament segments separated by small stripes in which the filaments are highly bent. The darkness of the bent regions corresponds to lesser filament density. Order parameter variation is shown as a gray sinusoidal curve and is directly correlated with density heterogeneities and filament bending.

The low values of the order parameter in alternating stripes can also be explained by lesser nematic alignment and, from the comparison images, are seen to correspond to the less dense regions of highly bent filament segments. The decreased density and the high curvature of the polymer contours result in more space between the filaments. Less tightly packed filaments result in a lesser ordering by the packing argument presented above. Bending therefore accounts for the small dark stripes observed at the boundaries of the areas of different alignments in polarization images, as well as for the dark stripes in fluorescence images.

The demonstrated correlations between periodic variations in director distortion, filament segment density, filament segment configuration, and local order parameter result in a more detailed description of the so-called zebra stripe patterns than have been previously presented [24,26]. These correlations are depicted in Fig. 10. From this diagram, it can be seen that in contrast to a simple zigzag pattern, highly bent regions between the stripes of alternating director appear, accounting for density and order parameter variations. It clearly shows that the zebra stripes do not represent discontinuities, but rather large smooth distortions in the direction of the nematic director.

B. Causal mechanisms of zebra stripe patterns

1. Coupling to active reaction kinetics

The results presented here show that the mechanism responsible for the formation of zebra stripe patterns in highly concentrated actin samples under the conditions studied does not involve the coupling of active reaction kinetics to distor-

tions in the direction of the nematic director. Evidence was not seen for either of the two potential mechanisms by which this coupling might occur. In the case of the first mechanism, that of instabilities generated by energy consumption via treadmilling, this result supports the conclusion of a previous study by Coppin and Leavis [24]. Thermodynamic equilibrium in these systems is likely hindered by filament entanglement and jamming at high concentrations. Therefore, the assumption that the system must relax to an undistorted state may not apply. The high viscosity and long relaxation times lead to both a strong dependence of alignment within the sample on mechanical stress and the unusual stability of the resulting textures [27,43].

Our results also show that the second mechanism, in which growing filaments jam against one another and buckle, also does not apply under our conditions. This result would seem to contradict other studies in which similar patterns were found to grow via this mechanism [24,45]. The absence of effects due to polymerization kinetics in our system, however, makes sense in light of the different sample conditions. Coppin *et al.*, studied F-actin solutions but used much lower actin concentrations and added gelsolin for filament nucleation; both of which significantly reduce the polymerization rate to a value low enough that competition between growth and ordering could be significant. More recently, experiments with microtubules in which growing filaments jam, accumulate stress, and buckle to produce remarkably similar patterns have been extensively studied [45,53]. Polymerization rates in this system too were presumably much lower than in ours. In both cases, the growth or jamming hypothesis was supported by observation of patterns that appeared to grow or develop on an observable time scale. In all cases, we were never able to observe the formation of the stripes and they appeared instantaneously under our experimental conditions.

2. Relaxation of accumulated stress

The instantaneous appearance of zebra stripes in our experiments under all conditions considered leads us to conclude that the formative mechanism is related to mechanical stresses and flows induced during sample preparation. This is supported by experiments on samples prepared at low temperatures (Fig. 9) in which filaments may have been short enough such that they could align in large domains without the formation of patterns. Once they were subjected to mechanical stresses by pressing on the slide or short sonication, the patterns always appeared, clearly showing these stresses to be the causal mechanism. Our conclusion is also supported by the consistent appearance of patterns below the limit of intrinsic thermodynamic ordering of 75 μM. Below this limit, F-actin does order but primarily by means of mechanical stresses induced in the samples [27]. Short-lived flows and mechanical deformations, it should be noted, are extremely hard to avoid in the preparation of these samples and are known to account for many polycrystalline defects [27,31].

We further propose that pattern formation in which the stripes grow over an observable time scale and those that appear instantaneously as presented here share a common causal mechanism—relaxation of accumulated stress in the nematically aligned filaments. This mechanism can be understood through the application of analysis of stripe formation for the synthetic polymer poly(benzyl-D-glutamate) (PBDG) [35,54]. For sheared synthetic polymers, there are two cases for the appearance of stripes due to the relaxation of accumulated stress after cessation of shear. These are differentiated by the magnitude of the previous shear rate and result in different rates of band formation. Both are described by a two-dimensional kinetic mechanism for the lateral (perpendicular to flow) and longitudinal (parallel to flow) band growth rates.

In systems sheared at low rates, the lateral band length gradually increases with time as the system attempts to relax the elastic energy accumulated during deformations in the nematic [35,54]. In systems sheared at high rates, patterns are seen to form immediately after the cessation of flow. The difference in the characteristic time constants for band growth in the two directions of length and width become much larger at high shear rates and the bands very quickly reach an appreciable aspect ratio. This explains the observation that the time for band formation after the cessation of flow was found to decrease inversely proportional to the previous shear rate [32,34], as well as to the low critical shear rate necessary for stripe formation onset [54]. In addition, the time for band formation was also affected by viscosity in systems where it increases strongly with concentration, such as with hydroxypropyl cellulose (HPC).

This mechanism can also describe the two cases of zebra stripe formation observed in biopolymer systems. In both cases, their formation is due to the relaxation of accumulated stresses and they can be differentiated by the rate of formation of the bands or stripes. Important differences in the nature of the stresses exist, however. We propose that the low shear case fits to [24,45] due to the observable stripe growth. In this case, there is a coupling to active reaction kinetics in which the gradual accumulation of the *internally* generated stress of filament growth is relaxed via buckling. This corresponds to a slow lateral band growth rate that is comparable to the longitudinal rate. The growing filaments jam and cannot rearrange and thus buckle to relax the stress.

Additionally, we conclude that the high shear case fits to our experiments due to the immediate appearance of the stripes after shearing induced in sample formation. In this case, stress is rapidly accumulated *externally* by an imposed shear and is relaxed via buckling of the nematic once the shear has ceased. This corresponds to a fast lateral band growth rate, which is much greater than the longitudinal rate. The high viscosity of these solutions containing long filaments insures that imposed shear stresses are also quite high, significantly stretching or distorting the nematic. In analogy to the high shear rate case for PDBG, we further propose that buckling results from contraction of nematically aligned filaments stretched during shear flows.

3. Buckling in F-actin solutions

In order to understand buckling of nematic F-actin due to contraction after shear-induced stretching, one must consider the importance of these polymers' length, semiflexibility, and

highly compressible nature in solution. Unique effects due to these properties can be understood qualitatively on an individual (but still strongly interacting) polymer level by a description of the system as it attempts to recover from the flow-induced distortion. In this scenario, the flow serves to set the initial condition and then plays no further role.

We propose that the coupling of density and orientation, as well as the compressible nature of the semiflexible filaments in solution, is the origin of zebra stripe formation. This coupling was initially introduced by de Gennes [55], who considered long semiflexible strongly extended polymers in solution under dilation due to splay deformations. Under such conditions, a strong coupling exists between concentration c and orientation $\mathbf{n}$. Due to this coupling, a deformation imposes local changes in the density and requires large energies. The resulting coupling to polymer density and compressibility in solution has been considered elsewhere [56,57] and it has been shown that linearized elasticity theory fails for such cases [58]. A full theoretical treatment based on these ideas and applied to the experiments presented here is therefore beyond the scope of this study and will be presented in a separate work in the near future.

Despite the lack of a full theoretical description, insight into the buckling response of the nematically aligned polymers can be gained by a simple qualitative consideration of the semiflexible nature of the filaments. This insight is gained by considering the energy cost incurred when they are stretched by a shear flow. Filaments in the unstretched state, although nematically aligned, still display transverse displacement, i.e., bends, that can be thought of as "stored length" along the filament contours. Flow-induced shear stretches the filaments, pulling out much of this stored length. After cessation of the shear, the filaments attempt to regain the stored length through transverse displacements or bends along the contours. Strong interfilament interactions between the close-packed filaments or bundles result in coordinated buckling and an overall warping of the nematic. By such means, patterns are formed by periodic bending at some characteristic wavelength, similar to those described in [45].

A plausible mechanism for the observed periodic density differences coupled to those of orientation and bending can also be related to the energetic cost of filament bending. Distortions of the nematic polymers have an associated energy cost described by the Frank elastic energy, whose constants grow with increasing concentration [55]. In order to minimize this cost, filament segments become more tightly packed in the straight regions as opposed to those with large bends. In this way, a deformation energy penalty is not invoked in the most highly concentrated areas and the free energy of the system is lowered for long-wavelength distortions. This description of the origin of the density heterogeneities is supported by the observation that they appear even for very short labeled filaments which presumably are small enough that they could be evenly distributed among the stripes in the patterned areas (Fig. 7). A full quantitative treatment of the coupling of density heterogeneities to director distortions, order parameter variations, and the energetic costs of filament bending is forthcoming.

V. CONCLUSION AND OUTLOOK

Our findings show that F-actin solutions in confined geometries are highly unstable to mechanical perturbations that produce zebra stripe patterns. These striped domains show periodic variations not only in the direction of the nematic director, but also in the density of the filament distribution, the magnitude of the order parameter, and the filament segment configuration. Comparison of polarization and fluorescence microscopy techniques shows that filaments undergo large angle bends and that bent regions correspond to areas of low nematic order and decreased filament density, whereas highly ordered regions contain very straight filament segments with a higher comparative density.

The formation of striped patterns due to relaxation buckling could potentially occur in active nematic systems as well. These systems have attracted much theoretical attention recently, resulting in a comprehensive description of instabilities that arise due to active motor activity in the polymer liquid crystals [59,60]. Internally generated flows are also possible in these systems [60,61], which could effectively operate in a similar fashion as the externally imposed flows during sample preparation presented here. In addition, cytoplasmic streaming in cells [62] could also act upon cytoskeletal filament networks in a similar manner. In both cases, stripes may form after cessation of flow due to these causes. It would be interesting to explore this possibility experimentally with active systems by the addition of motors to nematic actin solutions, better approximating a physiologically relevant cytoskeletal model.

ACKNOWLEDGMENTS

We would like to thank S. Ramaswamy, J. Prost, Björn Stuhrmann, and D. Strehle for helpful discussions. We acknowledge funding by the Alexander von Humbolt Foundation through the Wolfgang Paul Preis, the Deutche Forschungsgemeinschaft via research group 608, and Active Biomics Contract No. NMP4-CT-2004-516989.

[1] D. Pantaloni, C. L. Clainche, and M.-F. Carlier, Science **292**, 1502 (2001).
[2] T. Pollard and G. G. Borisy, Cell **112**, 453 (2003).
[3] M.-F. Carlier, C. L. Clainche, S. Wiesner, and D. Pantaloni, BioEssays **25**, 336 (2003).
[4] J. Bartles, Curr. Opin. Cell Biol. **12**, 72 (2000).
[5] D. A. Head, A. J. Levine, and F. C. MacKintosh, Phys. Rev. Lett. **91**, 108102 (2003).
[6] M. Gardel, J. Shin, F. MacKintosh, P. Mahadevan, P. Matsudaira, and D. Weitz, Science **304**, 1301 (2004).
[7] E. Atilgan, D. Wirtz, and S. Sun, Biophys. J. **90**, 65 (2006).
[8] P. Hotulainen and P. Lappalainen, J. Cell Biol. **173**, 383

(2006).
[9] Y. Aratyn, T. E. Schaus, E. W. Taylor, and G. G. Borisy, Mol. Biol. Cell **18**, 3928 (2007).
[10] D. Sept, J. Xu, T. Pollard, and J. McCammon, Biophys. J. **77**, 2911 (1999).
[11] O. Kratky and G. Porod, Recl. Trav. Chim. Pays-Bas **68**, 1106 (1949).
[12] L. Landau and E. Lifschitz, *Statistical Physics* (Addison-Wesley, Reading, MA, 1958).
[13] K. Kroy and E. Frey, Phys. Rev. Lett. **77**, 306 (1996).
[14] J. Wilhelm and E. Frey, Phys. Rev. Lett. **77**, 2581 (1996).
[15] J. Käs, H. Strey, J. X. Tang, D. Finger, R. Ezzell, E. Sackmann, and P. Janmey, Biophys. J. **70**, 609 (1996).
[16] L. L. Goff, O. Hallatschek, F. Amblard, and E. Frey, Phys. Rev. Lett. **89**, 258101 (2002).
[17] F. Gittes, B. Mickey, J. Nettleton, and J. Howard, J. Cell Biol. **120**, 923 (1993).
[18] H. Isambert and A. Maggs, Macromolecules **29**, 1036 (1996).
[19] L. Landau and D. T. Haar, *Collected Papers* (Gordon and Breach, New York, 1965).
[20] P. de Gennes and J. Prost, *The Physics of Liquid Crystals*, 2nd ed., International Series of Monographs on Physics (Oxford University Press, New York, 1993).
[21] M. Doi and S. Edwards, *The Theory of Polymer Dynamics*, International Series of Monographs on Physics (Oxford University Press, New York, 1988).
[22] A. Kerst, C. Chmielewski, C. Livesay, R. Buxbaum, and S. Heidmann, Proc. Natl. Acad. Sci. U.S.A. **87**, 4241 (1990).
[23] A. Suzuki, T. Maeda, and T. Ito, Biophys. J. **59**, 25 (1991).
[24] C. Coppin and P. Leavis, Biophys. J. **63**, 794 (1992).
[25] R. Furukawa, F. Kundra, and M. Fechheimer, Biochemistry **32**, 12346 (1993).
[26] P. Das, J. Roy, N. Chakrabarti, and U. Das, J. Chem. Phys. **116**, 9028 (2002).
[27] E. Helfer, P. Panine, M.-F. Carlier, and P. Davidson, Biophys. J. **89**, 543 (2005).
[28] P. W. Oakes, J. Viamontes, and J. X. Tang, Phys. Rev. E **75**, 061902 (2007).
[29] J. Viamontes, P. W. Oakes, and J. X. Tang, Phys. Rev. Lett. **97**, 118103 (2006).
[30] J. Viamontes and J. X. Tang, Phys. Rev. E **67**, 040701(R) (2003).
[31] K. Wissbrun, J. Rheol. **25**, 619 (1981).
[32] G. Kisst and R. Porter, Mol. Cryst. Liq. Cryst. **60**, 267 (1980).
[33] E. Marsano, L. Carpaneto, and A. Ciferri, Mol. Cryst. Liq. Cryst. **158**, 267 (1988).
[34] J. Gleeson, R. Larson, D. Mead, G. Kiss, and P. Cladis, Liq. Cryst. **11**, 341 (1992).
[35] S. Picken, P. Moldenaers, S. Berghmans, and J. Mewis, Macromolecules **25**, 4759 (1992).
[36] W. Song, S. Chen, Y. Jin, and R. Qian, Liq. Cryst. **19**, 549 (1995).
[37] J. Pardee and J. Spudich, J. Cell Biol. **93**, 648 (1982).
[38] R. Oldenbourg and G. Mei, J. Microsc. **180**, 140 (1995).
[39] K. Katoh, K. Hammar, P. Smith, and R. Oldenbourg, Mol. Biol. Cell **10**, 197 (1999).
[40] J. Käs, H. Strey, and E. Sackmann, Nature (London) **368**, 226 (1994).
[41] D. Smith, F. Ziebert, D. Humphrey, C. Duggan, M. Steinbeck, W. Zimmermann, and J. Kaes, Biophys. J. **93**, 4445 (2007).
[42] R. Oldenbourg, E. Salmon, and P. Tran, Biophys. J. **74**, 645 (1998).
[43] J. Viamontes, S. Narayanan, A. R. Sandy, and J. X. Tang, Phys. Rev. E **73**, 061901 (2006).
[44] R. D. Kamien, P. Le Doussal, and D. R. Nelson, Phys. Rev. A **45**, 8727 (1992).
[45] Y. Liu, Y. Guo, J. Valles, and J. Tang, Proc. Natl. Acad. Sci. U.S.A. **103**, 10654 (2006).
[46] D. Drenckhahn and T. Pollard, J. Biol. Chem. **261**, 12754 (1986).
[47] C. Zimmerle and C. Frieden, Biochemistry **25**, 6432 (1986).
[48] P. Niranjan, J. Forbes, S. Greer, J. Dudowicz, K. Freed, and J. Douglas, J. Chem. Phys. **114**, 10573 (2001).
[49] F. Oosawa and S. Asakura, *Thermodynamics of the Polymerization of Protein* (Academic, London, 1975).
[50] M.-F. Carlier, J. Biol. Chem. **266**, 1 (1991).
[51] T. Odijk, Macromolecules **19**, 2313 (1986).
[52] J. Tang, T. Ito, T. Tao, P. Traub, and P. Janmey, Biochemistry **36**, 12600 (1997).
[53] Y. Guo, Y. Liu, J. Tang, and J. Valles, Phys. Rev. Lett. **98**, 198103 (2007).
[54] J. Vermant, P. Moldenaers, and J. Mewis, J. Rheol. **38**, 1571 (1994).
[55] P. de Gennes, Mol. Cryst. Liq. Cryst. **34**, 177 (1977).
[56] T. Odijk, Liq. Cryst. **1**, 553 (1986).
[57] J. V. Selinger and R. F. Bruinsma, Phys. Rev. A **43**, 2910 (1991).
[58] J. Toner, Phys. Rev. Lett. **68**, 1331 (1992).
[59] R. Aditi Simha and S. Ramaswamy, Phys. Rev. Lett. **89**, 058101 (2002).
[60] Y. Hatwalne, S. Ramaswamy, M. Rao, and R. A. Simha, Phys. Rev. Lett. **92**, 118101 (2004).
[61] R. Voituriez, J. F. Joanny, and J. Prost, Phys. Rev. Lett. **96**, 028102 (2006).
[62] D. Bray, *Cell Movements*, 2nd ed. (Garland, New York, 2001).